ADVANCED BIOLOGY
www.advanced-bio.com

Xenogenic Neural Stem Cell-Derived Extracellular Nanovesicles Modulate Human Mesenchymal Stem Cell Fate and Reconstruct Metabolomic Structure

Burak Derkus, Melis Isik, Cemil Can Eylem, Irem Ergin, Can Berk Camci, Sila Bilgin, Caglar Elbuken, Yavuz Emre Arslan, Merve Akkulak, Orhan Adali, Fadime Kiran, Babatunde O. Okesola, Emirhan Nemutlu, and Emel Emregul*

Extracellular nanovesicles, particularly exosomes, can deliver their diverse bioactive biomolecular content, including miRNAs, proteins, and lipids, thus providing a context for investigating the capability of exosomes to induce stem cells toward lineage-specific cells and tissue regeneration. In this study, it is demonstrated that rat subventricular zone neural stem cell-derived exosomes (rSVZ-NSCExo) can control neural-lineage specification of human mesenchymal stem cells (hMSCs). Microarray analysis shows that the miRNA content of rSVZ-NSCExo is a faithful representation of rSVZ tissue. Through immunocytochemistry, gene expression, and multi-omics analyses, the capability to use rSVZ-NSCExo to induce hMSCs into a neuroglial or neural stem cell phenotype and genotype in a temporal and dose-dependent manner via multiple signaling pathways is demonstrated. The current study presents a new and innovative strategy to modulate hMSCs fate by harnessing the molecular content of exosomes, thus suggesting future opportunities for rSVZ-NSCExo in nerve tissue regeneration.

1. Introduction

Neurogenic differentiation is a dynamic process involving functional regulation of FoxO1,[1] EZH2-mediated histone methylation by SOX19b,[2] binding of neurotrophins to receptor tyrosine kinases (RTKs),[3] regulation of Rho-GDIγ by hepatic nuclear factor (HNF4-1), and myc-associated zinc finger protein (MAZ-1).[4] Also, the induction of NGN2 expression by PAX6 is well-known to promote neuronal differentiation by repressing HES5 and inhibiting downstream Notch effectors.[5] Moreover, STAT3 and SMAD1 activation by interleukin-6 family that induces glial protein expression plays an important role in neurogenic differentiation.[6]

B. Derkus
Stem Cell Research Lab, Department of Chemistry
Faculty of Science
Ankara University
Ankara 06560, Turkey
E-mail: burakderkus@gmail.com, bderkus@ankara.edu.tr

B. Derkus, M. Isik, C. B. Camci, S. Bilgin, E. Emregul
Interdisciplinary Research Unit for Advanced Materials (INTRAM)
Department of Chemistry, Faculty of Science
Ankara University
Ankara 06560, Turkey

C. C. Eylem, E. Nemutlu
Analytical Chemistry Division, Faculty of Pharmacy
Hacettepe University
Ankara 06530, Turkey

I. Ergin
Department of Surgery, Faculty of Veterinary Medicine
Ankara University
Turkey

C. Elbuken
UNAM-National Nanotechnology Research Center, Institute of Materials Science and Nanotechnology
Bilkent University
Ankara 06800, Turkey

The ORCID identification number(s) for the author(s) of this article can be found under https://doi.org/10.1002/adbi.202101317.

DOI: 10.1002/adbi.202101317

C. Elbuken
Faculty of Biochemistry and Molecular Medicine, Faculty of Medicine
University of Oulu
Oulu 90014, Finland

Y. E. Arslan
Regenerative Biomaterials Laboratory, Department of Bioengineering, Engineering Faculty
Canakkale Onsekiz Mart University
Canakkale 17100, Turkey

M. Akkulak, O. Adali
Department of Biological Sciences, Faculty of Science
Middle East Technical University
Ankara 06800, Turkey

F. Kiran
Department of Biology, Faculty of Science
Ankara University
Ankara 06560, Turkey

B. O. Okesola
Department of Eye and Vision Science
Institute of Life Course and Medical Sciences
Faculty of Medicine
University of Liverpool
Liverpool L7 8TX, UK

E. Nemutlu
Bioanalytic and Omics Laboratory, Faculty of Pharmacy
Hacettepe University
Ankara 06530, Turkey

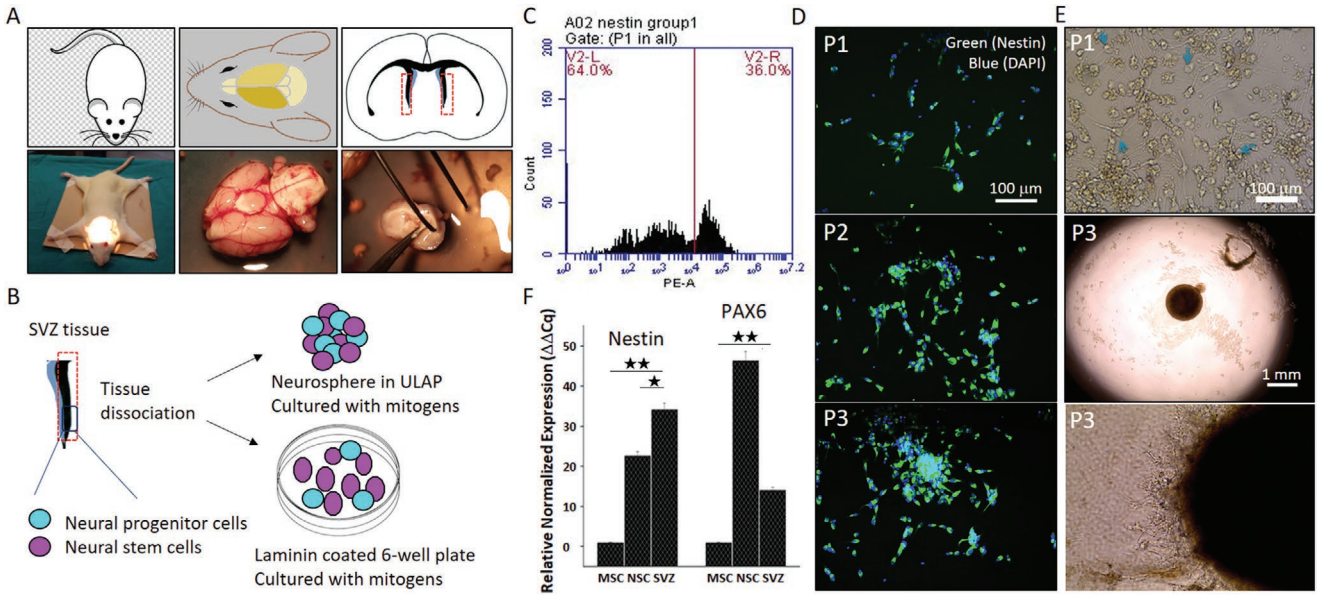

Figure 1. Isolation of rat subventricular zone (rSVZ)-derived neural stem cells (NSCs). A) Schematic representation and corresponding real images of the dissected rSVZ tissue. B) Illustration of NSC isolation from rSVZ tissue. C) Flow-cytometry diagram for Nestin+ NSCs. D) rSVZ-NSCs at passages 1, 2, and 3, stained with Nestin and DAPI. E) rSVZ-NSCs as monolayer culture (P1) and spheroid culture (P3). The cells when cultured onto Laminin-coated plate were shown to spread and form neuronal extensions. F) Gene expression study for Nestin and PAX6, two neural stem cell markers, in comparison to hMSCs (negative control) and rSVZ (positive control) (*$p < 0.05$, **$p < 0.01$). All experiments were performed thrice. Values represent means ± SEM ($n = 3$).

In addition to transcriptional and epigenetic regulation, post-transcriptional mechanisms, largely mediated by miRNAs, also contribute to cell specification during neural differentiation.[7,8] Several specific miRNAs are involved in different neurogenic processes such as neuronal migration,[9] proliferation of NSCs,[10,11] and neural cell specification.[12]

To induce neurogenic differentiation of mesenchymal stem cells (MSCs), inductive chemicals such as β-mercaptoethanol (βME) and retinoids have been demonstrated.[13] Growth factors, including epidermal growth factor (EGF), nerve growth factor (NGF),[14] and neurotrophins[15] have been prominently used to induce neurogenic gene expression. MSCs can also give rise to neural lineage cells and acquire neuronal phenotypes when induced with substances able to elevate intracellular level of cyclic adenosine monophosphate (cAMP). For example, forskolin and dibutyryl cAMP have been frequently used for neuronal differentiation of MSCs.[16] Despite the successful and continuous use of the aforementioned inductive factors, the use of growth factors and compounds are associated with certain drawbacks, including: i) poor solubility in aqueous solutions; ii) induction of autophagy and/or apoptosis;[17] iii) adverse cardiac remodeling;[18] and iv) adverse physiological action on the sensory and autonomic systems.[19] Consequently, an alternative approach to facilitate neurogenic differentiation of MSCs addressing such limitations will represent a breakthrough potential in the field.

Emerging evidence has implicated the use of exosomes in cell differentiation,[20,21] cellular communication,[22] disease diagnosis,[23] and tissue regeneration[24] as an attractive and viable strategy in cell/tissue engineering. Despite being a diverse source of bioactive proteins (growth factors), lipids, metabolites, and genetic materials (mRNAs, miRNAs, and noncoding RNAs)[25] that can stimulate cell differentiation, the use of exosomes to induce cellular differentiation and modulate fate decision has rarely been explored.[26–28] Glioma-derived exosomes,[26] exosomes isolated from neuronal cells,[27] and differentiating neuronal cells[28] have been shown to induce MSCs and NSCs into neuron-like cells. However, these early promising approaches only provided the formation of neuritic extensions with a low yield that is far from a complete induction and differentiation. Exosome-mediated induction strategy has also been harnessed to induce MSCs into other tissue-specific cells including adipose and bone,[29] nucleus pulposus,[30] and odontogenic[31] cells. However, the underlying complex molecular mechanisms of exosome-triggered stem cell differentiation have not been fully elucidated. Hence, there is an available strategy to achieve stem cell differentiation via exosomes by regulating fate-decision. This study for the first time reports that miRNA contents of primary cell-derived exosomes and the corresponding tissues are highly similar. Leveraging this molecular similarity, xenogenic primary cell-derived exosomes are reported to have the potential to modulate hMSCs fate, which, to our knowledge, has not been convincingly demonstrated to date.

Here, we use exosomes isolated from rat subventricular zone (rSVZ)- derived NSCs (rSVZ-NSCExo) to induce hMSCs into specific neural subtype cells due to their concentrated and innate biochemical contents and unique attributes. NSCs-derived exosomes have been shown to regulate neurogenesis,[32] attenuate apoptosis, and neuroinflammation.[33] It is well documented that NSCs in the SVZ regulate microglial morphogenesis in the central nervous system.[34] Considering this, we reasoned that primary NSCs-derived exosomes might induce hMSCs differentiation into different neurogenic lineage cells. Herein, we report a growth factor/cytokine-free strategy for the xenogeneic exosome-mediated induction of hMSCs. This induction strategy enables a reliable neurogenic induction with

a higher yield cell differentiation compared to previous reports, and enables the induction of hMSCs differentiation into different subtypes of neural cells in a dose-dependent manner.

2. Results and Discussion

2.1. Rationale of the Study

It is well-known that the therapeutic benefits of stem cells are largely driven by their paracrine factors. Increasing evidence showed that exosomes derived from stem cells might be the major source of these paracrine factors. Therefore, understanding the inductive capability of exosomes in various subtype of stem cells is highly sought after. Our strategy aims to characterize the molecular components and biological potentials of rSVZ-NSCs derived exosomes and to harness the innate biochemical cues to induce hMSCs differentiation into neural lineage cells as well as to modulate hMSCs fate with a reliable method. Exosomes were collected from xenogenic NSCs which we isolated from rSVZ (**Figure 1**A,B). After a comprehensive characterization process including miRNA profiling, rSVZ-NSCExo was used for the induction of hMSCs. Herein, we hypothesized that rSVZ-NSCExo can trigger neurogenic mRNA expression in hMSCs employing their genetic materials including miRNAs. Also, they can switch fibroblastic morphology to the unique morphologies of neural cells by employing the protein content of rSVZ-NSCExo that regulates neurogenesis. As such, we believe that rSVZ-NSCExo holds great potentials as a better substitute for pure growth factors and cytokines in regenerative medicine.

2.2. Isolation and Characterization of NSCs

To identify rSVZ derived NSCs, we carried out flow cytometry analysis for Nestin. It was quantitatively shown that 36% of the isolated SVZ-derived cells were Nestin-positive (Figure 1C). This isolation yield was found similar to those previously reported.[35,36] Immunofluorescence (IF) staining for Nestin further confirmed that the isolated cells have the characteristic phenotype of NSC (Figure 1D). The density of Nestin+ cells at the first passage was very low due to the presence of other neural-lineage cells, however, the density of Nestin+ cells increases with increasing passage number. In the third passage, almost all the cells exhibited Nestin+ phenotype (Figure 1D). This is possibly resulted from the elimination of non-neural stem cells because of their low proliferating capability. In addition to the flow cytometry and immunocytochemistry results, the ability of the isolated cells to form neurosphere was assessed. We observed the production of neurospheres (diameter ≈1 mm) when the isolated cells were cultured in N2B27 medium supplemented with basic fibroblast growth factor (bFGF) and EGF, which further confirmed the identity of the isolated cells (Figure 1E). When the obtained neurospheres were cultured with hMSCs on Laminin/poly-L-ornithine-coated wells in N2B27 in the absence of bFGF and EGF, formation of extended neurite-like branches (Figure 1D) that is characteristic of neuronal differentiation was observed. We then carried out gene expression analysis to probe the expression of two NSC-specific genes, Nestin and PAX6. NSCs exhibited a high-level expression for both Nestin and PAX6 when compared to the negative control hMSCs (Figure 1F). Unsurprisingly, the expression level of Nestin in SVZ tissue was higher than NSCs.

2.3. Characterization of rSVZ-NSCExo

The total protein content of rSVZ-NSCExo, isolated through the conventional serial ultracentrifugation (**Figure 2**B), was calculated to be 5 mg mL^{-1}. The transmission electron microscopy (TEM) micrograph of rSVZ-NSCExo showed many cup-shaped and stained wall nanovesicles with diameters between 50 and 200 nm, which is a typical size range for exosomes (Figure 2B). The TEM micrograph was consistent with the dynamic light scattering (DLS) data, which confirmed that rSVZ-NSCExo have a mean diameter of 80 nm (Figure 2C). The presence of two ubiquitous exosomal surface proteins (CD9 and CD63),[29,37] which were detected by immunoblotting, further proved the identity of rSVZ-NSCExo (Figure 2D).

The uptake of exosomes by the cells is an important parameter for an efficient induction and cell reprogramming. Hence, we assessed the uptake of rSVZ-NSCExo by hMSCs by co-culturing PKH67-labeled exosomes with hMSCs. The green fluorescence signal of PKH67-labeled exosomes was apparent 30 min after the injection of exosomes (Figure 2E). At this time point, individual exosomes or exosomal aggregates were recognizable. Also, an intense signal resulting from excessive uptake after 60 min was observed. These findings are consistent with the previous studies that reported the kinetics of exosomes' cellular uptake.[38,39] This cellular uptake is vital for an efficient paracrine effect of the exosomes.

2.4. Exploring the Molecular Content of rSVZ-NSCExo

Elucidation of the biomolecular content of exosomes derived from primary cells represents a useful strategy to identify the key biomolecular component that drives specific cellular processes under physiological conditions. To this end, we sought to determine the similarity between miRNA profiles of rSVZ tissue and rSVZ-NSCExo.

Hierarchical clustering (Figure 2F) and scattering (Figure 2G) analyses showed a significant overlap in the miRNA expressions of both rSVZ tissue and rSVZ-NSCExo (684 miRNAs). Some rat origin miRNAs (28 out of 728 miRNAs) in both cases were determined to be significantly up/down-regulated (change ≥twofold, $p \leq 0.05$, listed in Table S1, Supporting Information). This finding suggests that the isolated exosomes reflect the innate miRNA content of rSVZ tissue and can be used in cell induction. To the best of our knowledge, this result shows for the first time that miRNA contents of exosomes and the corresponding tissues are highly similar. We then performed gene ontology (GO) analysis for the significantly up/down-regulated miRNAs in conjunction with FunRich3.0 (Entrez IDs are presented in Table S2, Supporting Information) to show that the exosomes are enriched with nerve tissue-related miRNAs (Figure S1A, Supporting Information). Furthermore,

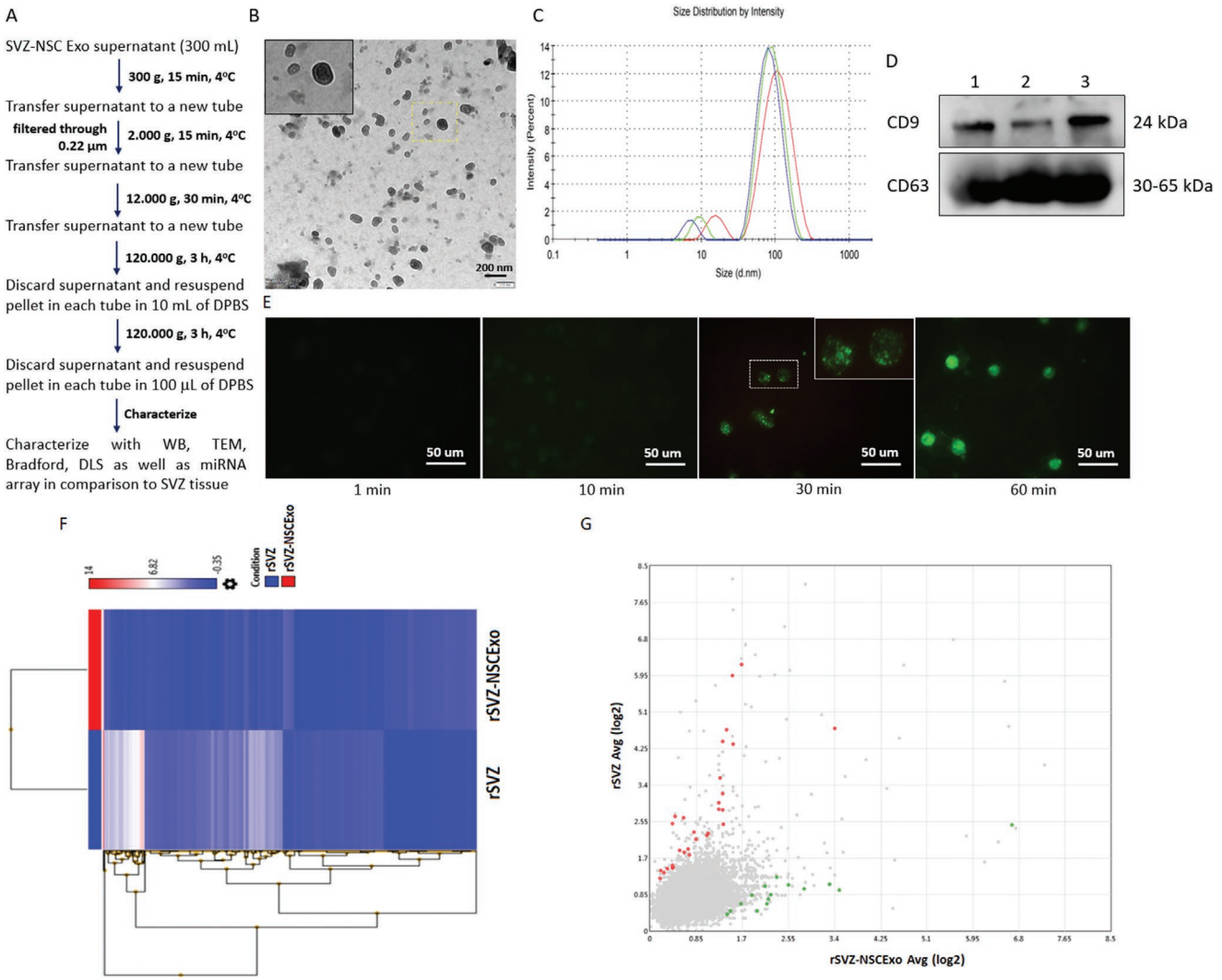

Figure 2. Isolation and characterization of rSVZ-NSCExo. A) The protocol applied to rSVZ-NSC conditioned media to isolate exosomes. B) TEM image showing the cup-shape exosomes with 50–200 nm diameter. C) DLS spectrum exhibiting the size distribution for rSVZ-NSCExo ($n = 3$). D) Immunoblotting bands for CD9 and CD63, two exosomal surface proteins. E) Tracking the time-dependent uptake of PKH67-stained rSVZ-NSCExo by hMSCs. F) Hierarchical clustering of miRNA profile of rSVZ-NSCExo in comparison to rSVZ tissue ($n = 3$). G) Scattering graph obtained with significantly differentially expressed miRNAs in rSVZ-NSCExo compared to rSVZ tissue ($n = 3$). Red and green dots represent highly expressed miRNAs in rSVZ and rSVZ-NSCExo, respectively.

the enriched miRNAs regulate different biological processes including cell communication, signal transduction, and regulation of nucleic acid metabolism (Figure S1B, Supporting Information) with receptor binding activity, GTPase activity, protein serine/threonine kinase activity, and transcription factor activity (Figure S1C, Supporting Information). This result is consistent with previous reports.[40,41]

To identify rSVZ-NSCExo-enriched metabolites prior to downstream applications, we performed a combined gas chromatography-mass spectrometry (GC-MS) and liquid chromatography-mass spectrometry (LC-MS) analysis. Amongst the whole metabolome, we identified 122 metabolites over the threshold (the list is available in Excel I file). Amongst the numerous metabolites, dopamine,[42] betain,[43] sphinganine,[44] cholesterol,[45] docosapentaenoic acid,[46] and hypotaurine[47] are known to take part in neurogenesis or neural system functions. This finding supports the miRNome data and implies that rSVZ-NSCExo carries innate neurogenic materials. The obtained metabolome data also strengthen our hypothesis questioning the neuro-inductive potential of rSVZ-NSC-derived exosomes.

2.5. Cell Biocompatibility of rSVZ-NSCExo

To assess the potential cytocompatibility of rSVZ-NSCExo, we conducted Calcein-AM and Ethidium Homodimer-1 (EthD-1) staining as well as 3-(4,5-dimethylthiazol-2-yl)-5-(3-carboxymethoxyphenyl)-2-(4-sulfophenyl)-2H-tetrazolium (MTS) testing for different doses of rSVZ-NSCExo (10, 50, and 100 µg mL^{-1}) to examine the cell viability and proliferation. Both microscopy (Figure S2A, Supporting Information) and MTS

assay (Figure S2B, Supporting Information) confirmed that rSVZ-NSCExo did not elicit an obvious cytotoxic effect when applied between 10–100 μg mL^{-1}. This concentration range is consistent with concentrations we tested for neurogenic induction of hMSCs.

2.6. rSVZ-NSCExo Induces hMSCs into Neuroglial or Neural Stem Cell Phenotype and Genotype in a Dose-Dependent Manner

Tissue-specific exosomes are enriched in RNAs and proteins able to influence cellular processes, just like transcription factors do, and thereby regulate stem cell fate.[29,48] Considering this, we hypothesized that exosomes obtained from rSVZ-NSCs contain numerous biomolecules that can induce cell differentiation or direct cell fate-decision. To test this hypothesis, we incorporated rSVZ-NSCExo (10, 50, and 100 μg mL^{-1}) into hMSCs medium and maintained the culture up to 10 days (**Figure 3**A). IF microscopy was used to probe two NSC markers (Nestin and SOX2), a neuroglial marker (GFAP), and a marker that is associated with the skeleton (vimentin). Morphological observations showed that a high level (100 μg mL^{-1}) of rSVZ-NSCExo switched the fibroblastic morphology of hMSCs into a less spread/more rounded morphology of NSCs (Figure 3B). The cells were highly Nestin+ (58%) and SOX2+ (64%) positive but exhibited lower level of GFAP+ (12%) morphology (Figure 3C). When the rSVZ-NSCExo concentration was reduced to 50 μg mL^{-1}, the percentage of Nestin+ and SOX2+ cells decreased to 36% and 45%, respectively. In contrast, the percentage of GFAP+ cells increased to 31%. Interestingly and unexpectedly, in the presence of a very low concentration of rSVZ-NSCExo (10 μg mL^{-1}), a massive increase in GFAP+ cells (45%) was observed, whereas the percentage of Nestin+ and SOX2+ cells was restrained with 31% and 24%, respectively. Similar to the observed neuro-inductive property of rSVZ-NSCExo, hMSCs cultured in N2B27 are highly differentiated into NSCs with high Nestin+ (70%), SOX2+ (69%) cell ratio and very low GFAP+ cell ratio (≈10%) as expected. On the other hand, hMSCs cultured in growth medium (GM) retained their fibroblastic phenotype. Overall, our results show that rSVZ-NSCExo regulates hMSCs' fate in a dose-dependent manner. In the light of previous studies,[49] we speculate that this lineage-specification results from the enriched exosomal content of rSVZ-NSCExo. NSC-specification derives from rSVZ-NSCExo's ability to transform cells where the exosomal content is sufficient at higher doses. On the other hand, at a lower dose, the cells undergo random differentiation. This observation suggests that hMSCs are induced by rSVZ-NSCExo in a dose-dependent manner. Similar results demonstrating exosome-mediated cell induction, but not modulation of cell fate, have been previously reported for autogenic exosomes.[50,51] Also, NSCs and glioma cell derived exosomes have previously been reported to induce astrocytic differentiation of stem cells.[26,52] In addition, exosome reporter mice have shown that exosomes play a significant role in intercellular communications between neurons and glial cells, and neurons secrete specific miRNAs-containing exosomes that upregulate astroglial glutamate expression.[53] In our approach, rSVZ-NSCExo seems to increase the differentiation of hMSCs into GFAP+ cells when applied in lower doses, implying that exosomes increase the gliosis. This finding is thought to have potential implications in the development of treatment methods or therapeutics for the treatment of astrocyte dysfunction diseases such as Alzheimer's, ALS, Huntington, or aging brain.

To corroborate the immunocytochemistry results, we investigated mRNA expression of neural markers (Nestin, SOX2, GFAP) in hMSCs following the induction with rSVZ-NSCExo. When we treated hMSCs with high dose of rSVZ-NSCExo (100 μg mL^{-1}), we observed a significant expression of Nestin (by 6.7-fold, $p < 0.05$) and SOX2 (by 3.1-fold, $p < 0.05$) relative to the non-treated hMSCs (**Figure 4**A). Remarkably, expression levels of Nestin and SOX2 following the treatment with rSVZ-NSCExo (100 μg mL^{-1}) were similar to those obtained by culturing the cells in the N2B27 medium (positive control). A decrease in the level of Nestin expressions was observed with decreasing concentration of rSVZ-NSCExo (50 μg mL^{-1}) by 1.1-fold, but the decrease was not significant ($p > 0.05$). However, SOX2 expression was decreased in rSVZ-NSCExo (50 μg mL^{-1}) treatment condition by 1.67-fold, indicating a significant change in SOX2 expression ($p < 0.05$). On the other hand, GFAP expression was noticeably upregulated only in the cells treated with a low dose of rSVZ-NSCExo (10 μg mL^{-1}). In contrast, hMSCs that were cultured in N2B27 did not exhibit GFAP expression. Surprisingly, the expressions of Nestin and SOX2 were found to be insignificantly lower in D10 when compared to D3, which might have resulted from Nestin+SOX2+ cell death or random differentiation of hMSCs-derived NSCs (Figure 4B). The GFAP expression was significantly higher by 1.43-fold ($p < 0.05$) on day 10 compared to day 3.

To optimize the rSVZ-NSCExo assisted induction of hMSCs into neural-lineage cells, we deeply investigated the optimal cell density and exosome loading protocol. To this end, rSVZ-NSCExo assisted induction protocol was applied to different initial cell densities (5×10^4, 1×10^5, and 2×10^5 cells per 6-well). In this case, we found that lowest initial cell density (5×10^4) provided the highest Nestin expression, and the level of expression was gradually decreased when cell density was increased (**Figure 5**A). On the other hand, the expression of SOX2 and PAX6 was insignificantly changed when cell density was increased to 1×10^5, whereas their expressions were seen to decrease when the cell density was further increased. Given the high rSVZ-NSCExo concentration (100 μg mL^{-1}) applied in these experiments, as expected, the expression of GFAP was not significant in all conditions. A similar result that showed the down-regulation of NSC-specific genes with increasing initial cell density has been reported.[54] This might also be attributed to the likelihood of a decreasing percentage of differentiated cells with increasing number of cells beyond an optimum density. To decipher the involvement of neuronal differentiation, which might be one of the reasons for the decreased expression level of NSC-specific genes, we investigated the expression of MAP2 in the same conditions. The expression of MAP2 was found significant (Figure 5A). To further explore the underlying factors for the perturbed neural gene expressions, we performed a gene expression analysis for vimentin, which is a class-III intermediate filament found in non-epithelial cells, especially mesenchymal cells. The expression of vimentin

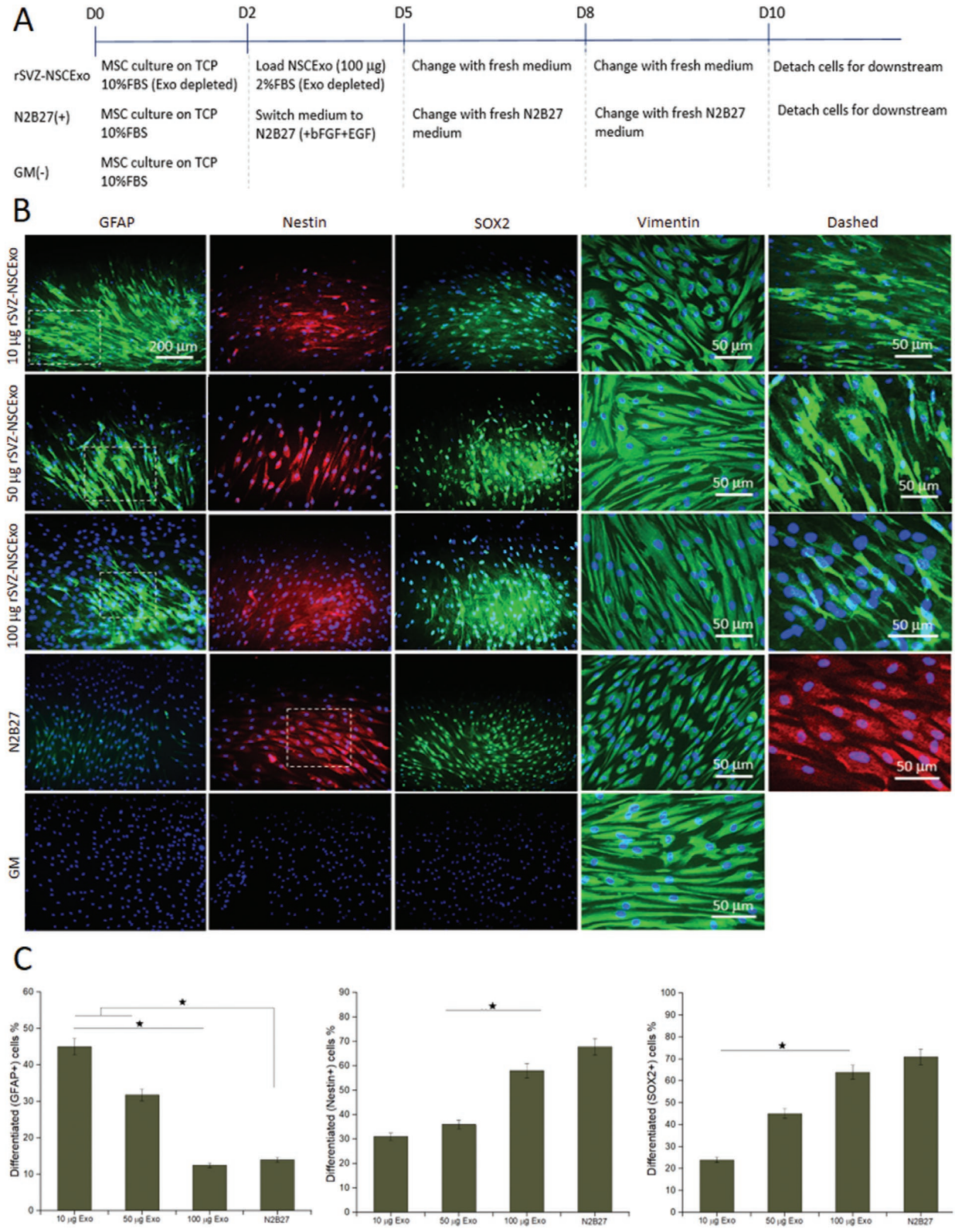

Figure 3. Characterization of cell induction through immunostaining. A) Overview of the culture system. B) Immunofluorescence staining of rSVZ-NSCs-induced (10, 50, and 100 µg mL^{-1}) hMSCs for glial (GFAP) and NSC markers (Nestin and SOX2). Vimentin staining was performed for the assessment of cell phenotypes. The cells induced with N2B27 medium were considered as positive control while non-treated hMSCs were used as negative control. C) The graphs indicate GFAP+, Nestin+, and SOX2+ cell ratios. Statistical significance was determined using a one-way ANOVA followed by Tukey's post hoc test (*$p < 0.05$).

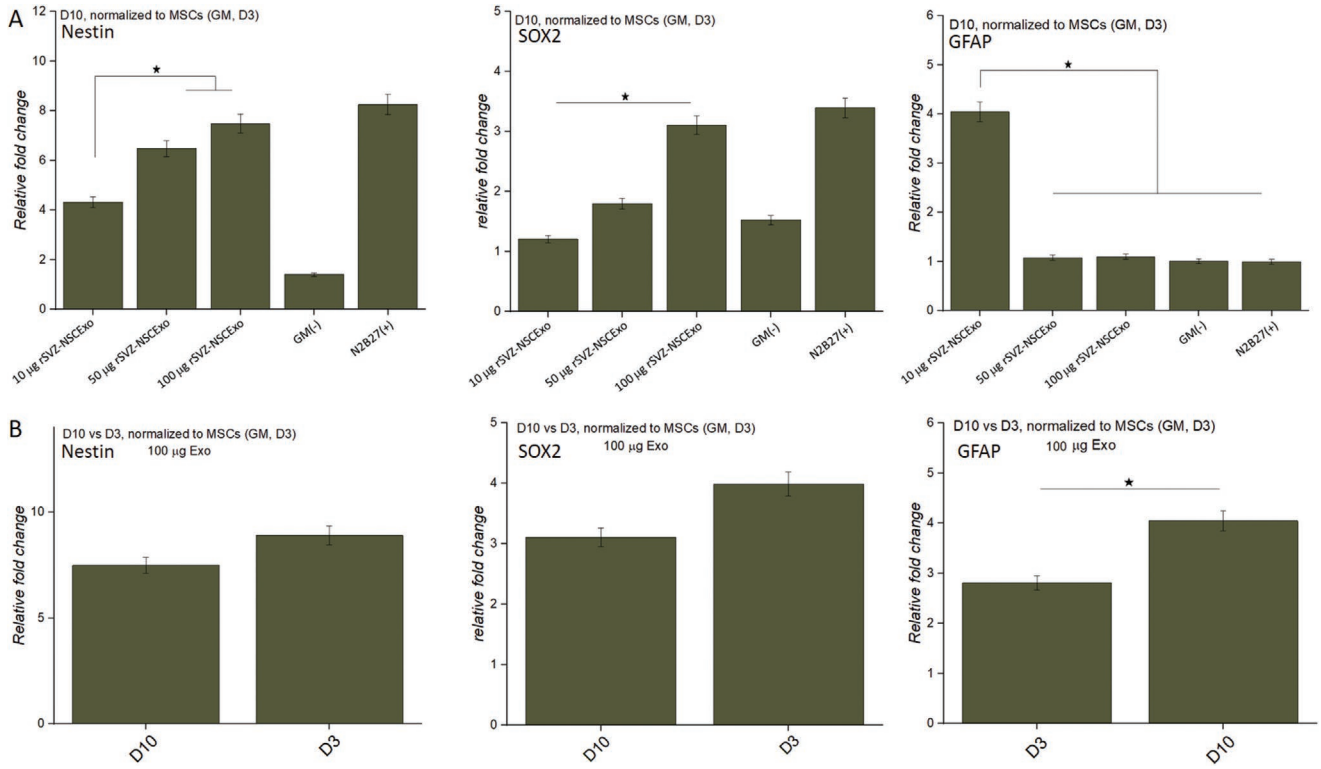

Figure 4. Characterization of neurogenic induction of hMSCs via rSVZ-NSCExo (n = 3, technical replicate = 3). A) RT-qPCR graphs related to the expressions of Nestin, SOX2, and GFAP (A). B) Alterations of Nestin, SOX2, and GFAP expressions with time. N2B27-induced hMSCs and non-treated hMSCs were used as positive and negative controls, respectively. Statistical significance was determined using a one-way ANOVA followed by Tukey's post hoc test (*$p < 0.05$).

appeared to be higher when the initial cell density was doubled from 5×10^4 to 1×10^5, indicating a higher mesenchymal character at the initial cell density of 1×10^5. Whereas, it decreased when the cell density was further increased (2×10^5). This decrease in vimentin expression in higher cell density might be due to contact inhibition.

To further validate the rSVZ-NSCExo assisted induction protocol, we evaluated the expressions of genes following the treatment of hMSCs with three different time intervals and loading regimes (Figure 5B). The results showed that expressions of all neural-lineage-specific genes were augmented by loading the rSVZ-NSCExo two times with 3 days' intervals (Figure 5C). Unexpectedly, after loading the rSVZ-NSCExo three times with 3 days' intervals, we observed a massive inhibition in neural gene expressions. Possibly, this inhibition in gene expressions originates from the over-saturation of cells with exosomes or exosomal contents (miRNAs and proteins) that trigger dysfunctional cellular behaviors.[55] Moreover, excessive amount of proteins might have led to inhibition of cell proliferation due to improper protein localization[56] and ER-stress.[57]

2.7. Temporal and Dose-Dependent Modulation of hMSCs by rSVZ-NSCExo: Understanding the Underlying Mechanism

To further corroborate the hypothesis, we obtained miRNA profiles of rSVZ-NSCExo (100 µg mL^{-1}) induced hMSCs in comparison with non-induced hMSCs. Hierarchical clustering and scattering graphs (**Figure 6**A,B) revealed that 54 miRNAs appeared to be significantly up/down-regulated in rSVZ-NSCExo treated hMSCs (listed in Table S3, Supporting Information). miR-3178, miR-1469, let-7b, miR-1915, miR-762, miR-3196, miR-1908, miR-2861, miR-149, miR-4281, miR-663, miR-3195, miR-4281, miR-663, miR-3195, miR-222, miR-20a, miR-1975, miR-1228, miR-320d, miR-24, miR-424, and miR-1268 were top 20 most highly up/down-regulated miRNAs. Reverse transcriptase-quantitative polymerase chain reaction (RT-qPCR) analysis conducted for the two most highly up-regulated and one down-regulated miRNA (miR3178, miR1469, and miR20a) confirmed the validity of differentially expressed miRNAs identified by microarray (Figure 6C). Some of the up-regulated miRNAs (miR-3178, miR-1915, miR149, miR-663, miR-222, miR-221, and miR-181) observed in this work are also characteristic features of embryonic stem cells differentiation into neural cells.[58] In addition, four miRNAs (miR-222, miR-1268, miR-181, and miR-4281) that were determined to be up-regulated in this study have been associated with neurogenic differentiation of periodontal ligament stem cells.[59] Many reports have showed that the expression of miR-181 increases with neurogenic differentiation.[60–62] Moreover, the up-regulated miR-24 in this work has been associated with neurogenic differentiation.[63] Up-regulation of these miRNAs in hMSCs after rSVZ-NSCExo induction resembles the neural differentiation process of human adult stem cells using standard inductive factors, thus showing potential of rSVZ-NSCExo as a promising substitute for conventional exogenous inductive factors.

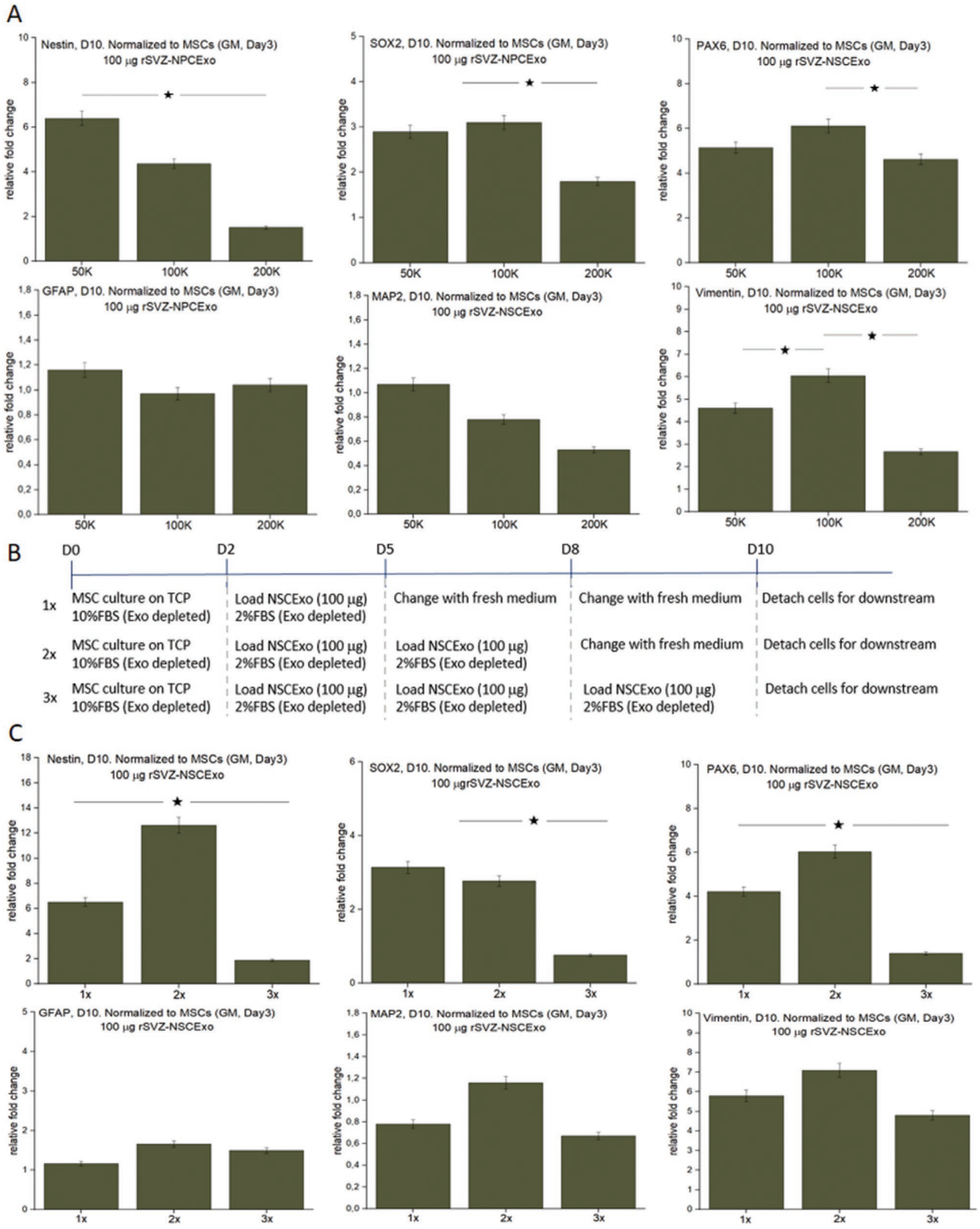

Figure 5. Optimization of cell induction. A) Effect of cell density (50, 100, and 200 K) on rSVZ-NSCExo mediated neurogenic differentiation of hMSCs. B) Schematic presentation of induction conditions. C) Effect of exosome loading frequency (1, 2, and 3 times with 3 days' intervals) on rSVZ-NSCExo mediated neurogenic differentiation of hMSCs. All experiments were performed thrice with technical replicates ($n = 3$). Statistical significance was determined using a one-way ANOVA followed by Tukey's post hoc test ($^*p < 0.05$).

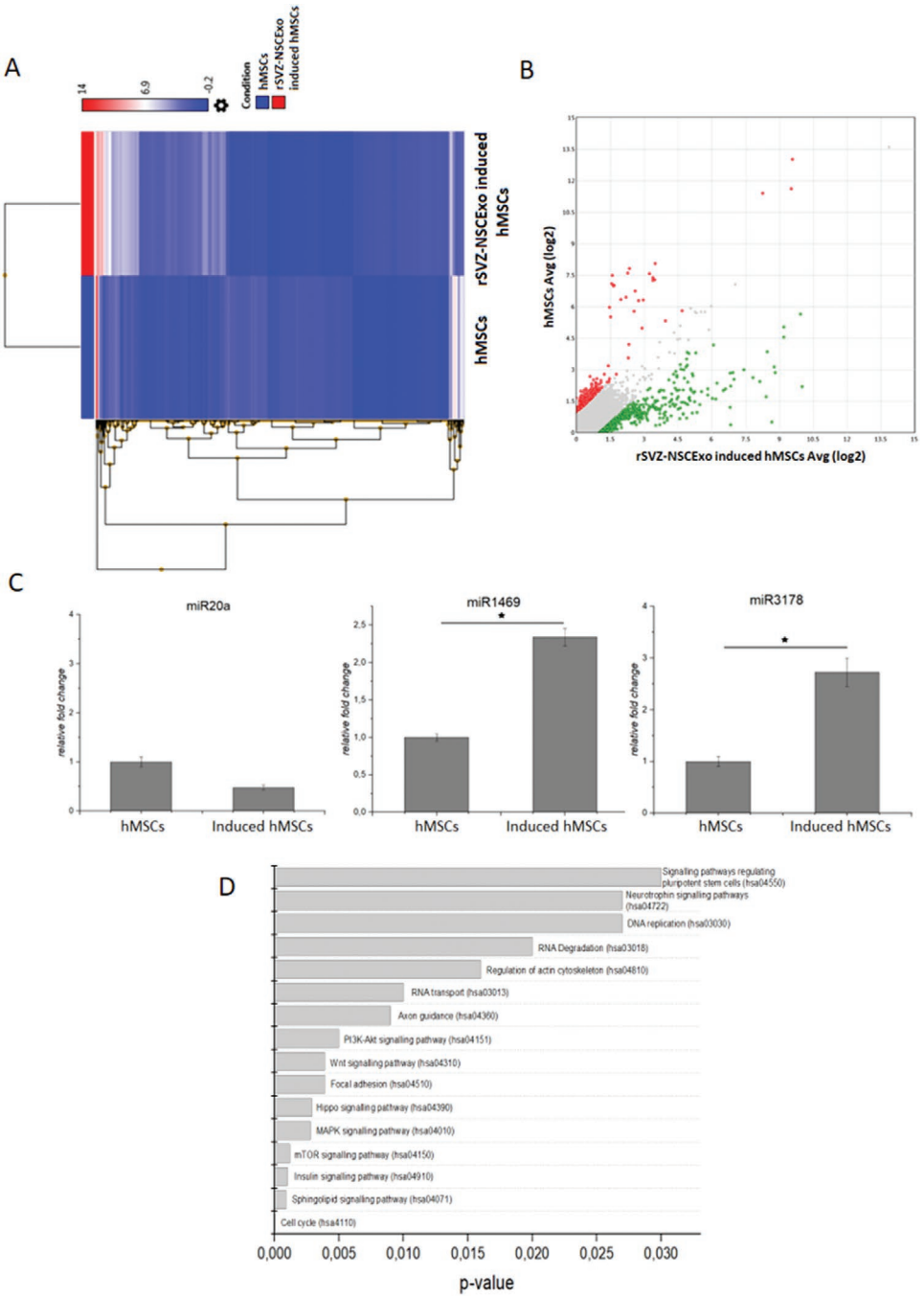

Figure 6. Assessment of the mechanism of action of rSVZ-NSCExo mediated cell induction by miRNA profilling. A) Hierachical clustering and B) scatter graph representing the significantly up/down regulated miRNAs in hMSCs after induction with rSVZ-NSCExo (100 µg mL^{-1}) for 10 days ($n = 3$). C) Validation of two overexpressed (miR1469 and miR3178) and one down-regulated (miR20a) miRNAs by RT-qPCR. Statistical significance was determined using a one-way ANOVA followed by Tukey's post hoc test (*$p < 0.05$). D) KEGG pathways obtained with significantly up/down regulated miRNAs in hMSCs induced with rSVZ-NSCExo (100 µg mL^{-1}) for 10 days.

Next, upregulated miRNAs were used to reveal the cellular pathways and processes regulated by the overexpressed miRNAs. For this, we utilized FunRich3.0 and mirPathV.3. GO analysis performed with FunRich3.0 showed that upregulated miRNAs within rSVZ-NSCExo display transcription factor activity ($p < 0.001$), transcription regulator activity ($p < 0.01$), and receptor binding activity ($p < 0.012$) (Figure S3, Supporting Information). Exosomal miRNAs affect the neurogenic differentiation process through regulating nucleic acid metabolism ($p < 0.01$) by interacting various transcription factors including EGR1 (p <0.001), SP1 ($p < 0.001$), SP4 ($p < 0.001$), POU2F1 ($p < 0.001$), SOX1 ($p < 0.001$), and RREB1 ($p < 0.001$) mainly in nucleus ($p < 0.001$) (Figure S3, Supporting Information). Moreover, GO analysis revealed that differentially expressed

miRNAs regulate these transcriptional factors through various pathways that include TRAIL signaling pathway ($p < 0.001$), IFN-g signaling pathway ($p < 0.001$), ErbB receptor signaling network ($p<0.001$), Glypican-1 network ($p < 0.001$), c-MET ($p < 0.001$), and PDGF receptor signaling pathway ($p < 0.001$) (Figure S3, Supporting Information). In addition to FunRich3.0, we performed a GO study using mirPathV.3 to reveal KEGG pathways affected by the rSVZ-NSCExo. The results revealed that the essential target genes of the differentially expressed miRNAs were Insulin, MAPK, Wnt, Hippo, PI3K/Akt, Axon guidance, RNA degradation, and neurotrophin signaling pathways (Figure 6D). To conclude, the GO study consolidated the microarray results and supported the idea that rSVZ-NSCExo, through their miRNA content, has functions in regulating neurogenic differentiation of hMSCs.

The target biological pathways of the differentially expressed miRNAs including IFN-g signaling pathway, ErbB receptor signaling network, glypican-1 network, c-MET, and PDGF receptor signaling pathway have previously been demonstrated to have functions in different stages of neurogenesis. IFN-g regulates the proliferation and differentiation of NSCs in SVZ,[64,65] while ErbB plays a critical role in neurogenic-specification and neuronal migration.[66,67] In addition, glypican-1 is expressed by NSCs[68] and controls various neurogenic processes over FGF signaling.[69] The c-MET mediates dendritic growth and synaptogenesis,[70] while PDGF initiates neuronal differentiation of SVZ progenitor cells.[71] Like our GO study, others have indicated that EGR1,[72] SP1,[73] SP4,[74] and SOX1[75] might be the underlying driver for transcript-level regulation of neural differentiation. Lastly, the use of miRPathV.3 reveals the KEGG pathways over which rSVZ-NSCExo mediated neural-specification occurs. The Wnt,[76] Hippo,[77] MAPK,[78] Neurotrophin,[79] and PI3K/Akt[80] pathways are believed to associate with neurogenic differentiation processes.

To deeply investigate the mechanism of action of rSVZ-NSCExo-mediated cell induction and ultimate functions of exosomes in hMSCs, we additionally employed another high-throughput screening method namely non-targeted metabolomics. In this case, we extracted metabolites from hMSCs that were induced with 10, 50, and 100 μg mL^{-1} rSVZ-NSCExo for 10 days, and the samples were subjected to combined GC-MS and LC-MS analyses. A total of 16351 mass features were detected by liquid chromatography quadrupole time-of-flight mass spectrometry (LC-qTOF-MS), amongst them, 77 and 15 metabolites were identified through LC-MS and LC-MS/MS, respectively. Additionally, 424 metabolites were detected, and 62 metabolites were identified by GC-MS (data available in Excel II). The partial least squares-discriminant analysis (PLS-DA) score plot showed a remarkable discrimination between metabolic phenotypes of the three groups (**Figure 7**A), which was further confirmed by one-way ANOVA (Figure S4, Supporting Information). This clear discrimination implies an altered metabolic structure in hMSCs when induced with different concentrations of rSVZ-NSCExo (10, 50, or 100 μg mL^{-1}). The most significantly altered 15 metabolites were presented in the variable importance in projection (VIP) (Figure 7B). The hierarchical cluster analysis of the metabolites further depicted the changes of these metabolites between the three groups (Figure 7C). The clear pattern during the transition from 10 to 100 μg mL^{-1} rSVZ-NSCExo is an indication of the change in metabolome in response to rSVZ-NSCExo dose.

In addition to dose dependency, we investigated the change in metabolite profiles at different time points (1, 3, 5, and 10 days) by keeping the 100 μg mL^{-1} rSVZ-NSCExo constant (data can be found in Excel II). The production of metabolites by cells varies with time with low intragroup variation (Figure 7D), confirmed by ANOVA test (Figure S5, Supporting Information). The most significantly altered metabolites were presented in VIP (Figure 7E), which include betaine, sorbose, myo-inositol, taurolithocholic acid, and serine, amongst others. The hierarchical clustering analysis obtained with most differentially altered metabolites demonstrated a pattern transition from day 1 to 10, asserting a temporal change in cell metabolome following the introduction of rSVZ-NSCExo (100 μg mL^{-1}) (Figure 7F). The significantly altered metabolites possibly perform their functions by affecting the pathways alanine, aspartate and glutamate metabolism, pantothenate and CoA biosynthesis, aminoacyl-tRNA biosynthesis, and citrate cycle (Figure 7G) (see Excel II) in addition to the pathways for organic cation/anion/zwitterion transport ($p = 0.0026$), transport of bile salts and organic acids, metal ions and amine compounds ($p = 0.0037$), glycerophospholipid catabolism ($p = 0.0067$), dopamine receptors ($p = 0.0079$), inositol transporters ($p = 0.0032$), dopamine neurotransmitter release cycle ($p = 0.038$), and sphingolipid de novo biosynthesis ($p = 0.048$) (obtained by Reactome.org). The interaction network of the enriched metabolites has been presented in Figure 7H. Dopamine, pyruvic acid, putrescine, taurine, and amino acids (e.g., serine, cysteine, hydroxyproline, phenyl alainine, etc.) exhibited maximum interactions with other metabolites indicating the maximum potential functional relationship with other metabolites in the network.

To conclude, metabolomics results are consistent with the observed phenotypic change upon induction of hMSCs with various concentrations of rSVZ-NSCExo. The alteration in metabolite profile was not only dose-dependent but reconstructed by cells in time (from the initial induction time to the end of the culture duration -10 days-). This time-dependent change in metabolite profile indicates that rSVZ-NSCExo drives a temporal modulation in hMSCs to generate the new phenotype. Similar temporal alterations in metabolite profiles have previously been reported for the differentiation of MSCs into osteoblasts,[81] specification of NSCs,[82] reprogramming of fibroblasts into induced pluripotent stem cells (iPSCs),[83] induction of iPSCs into hepatocyte-like cells,[84] and during myogenesis of skeletal muscle cells.[85]

3. Conclusion

Mesenchymal stem cells have generated a great amount of enthusiasm in the past decades as a novel therapeutic paradigm for a variety of tissue regeneration due to their inherent multiple biological properties. Traditionally, MSCs are cultured on a dish or materials scaffold and induced into tissue-specific cells by supplementation with cytokines, chemokines, and growth factors. The main challenge with these induction methods is whether growth-factor-induced cells resemble any stage of in vivo neurogenesis. Also, the reliability of the use

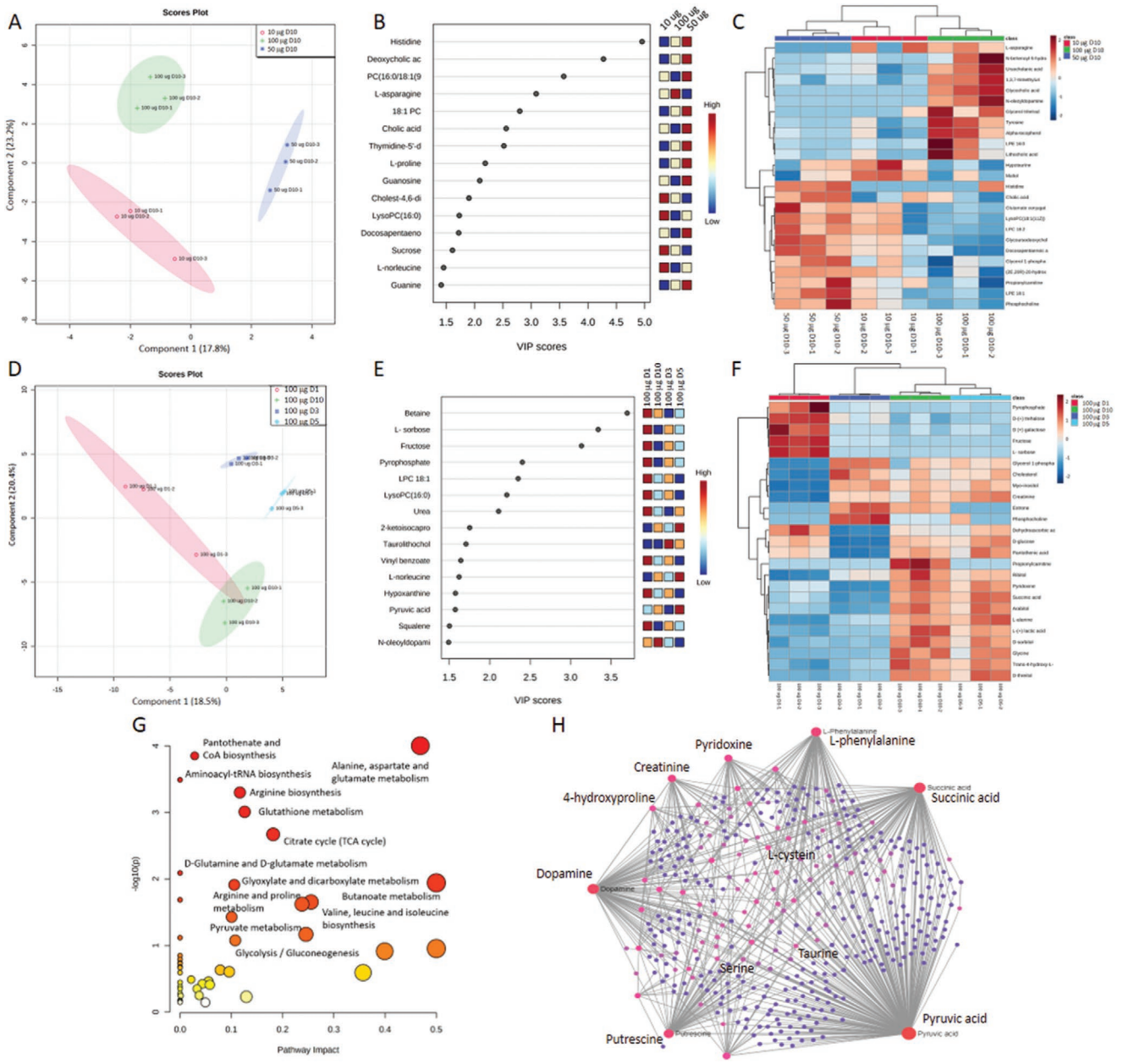

Figure 7. Untargeted metabolomics analysis for dose-dependent and temporal induction of hMSCs through rSVZ-NSCExo. A) PLS-DA diagram showing the discrimination in metabolite profile in hMSCs treated with 10, 50, and 100 µg mL^{-1} rSVZ-NSCExo. B) VIP score plot and C) hierarchical clustering analysis obtained by altered metabolites in hMSCs that were induced with 10, 50, and 100 µg mL^{-1} rSVZ-NSCExo. D) PLS-DA diagram indicating the inter-group discrimination in metabolite profile in hMSCs treated with 100 µg mL^{-1} rSVZ-NSCExo for 1, 3, 5, and 10 days. E) VIP score plot and F) hierarchical clustering heatmap graph that demonstrate the metabolite alteration patterns in hMSCs treated with 100 µg mL^{-1} rSVZ-NSCExo for 1, 3, 5, and 10 days. G) Pathway impact graph representing the most significantly affected pathways during induction process. H) Metabolite–metabolite interaction network revealing the molecular interactions during cell induction. The metabolites are represented as nodes (circles) highlighted in red in case of higher betweenness centrality followed by pink and blue in lower betweenness centrality. The size of the node indicates node degree (number of links a node has to other nodes). All analyses have been conducted by MetaboAnalyste. $n = 3$, technical replicate = 3.

of growth-factor-induced MSCs in regenerative medicine is questionable. To address these challenging issues, we examined the use of xenogenic exosomes obtained from rSVZ-derived primary NSCs in neural specification of hMSCs as a new strategy. We explored the dose-dependent and temporal modulation of hMSCs by rSVZ-NSCExo and their resulting molecular change at both miRNA and metabolite levels. The ability of rSVZ-NSCExo to switch hMSCs into neuroglial cell or neural stem cell phenotype and genotype largely depends on the dose of rSVZ-NSCExo. Given the GO study obtained with miRNome data, the neural specification process is seen to proceed mainly through neural system-related pathways that include Insulin, MAPK, Wnt, Hippo, PI3K/Akt, Axon guidance, RNA degradation, and neurotrophin signaling. In

addition, a broad-range of exosomal metabolites (e.g., dopamine, betain, sphinganine, cholesterol, docosapentaenoic acid, and hypotaurine) coordinately take part in neural specification by affecting a set of pathways (e.g., organic cation/anion/zwitterion transport, transport of bile salts and organic acids, metal ions and amine compounds, glycerophospholipid catabolism, dopamine receptors, inositol transporters, dopamine neurotransmitter release cycle, and sphingolipid de novo biosynthesis). Our study opens a new venue as a novel exosome-based platform capable of inducing MSCs to neural-specific cells for potential application in nerve regeneration in vivo.

4. Experimental Section

Isolation and Characterization of NSCs from rSVZ: NSCs were isolated from SVZ tissues[86] obtained from the brains of rats ($n = 9$) as previously described[87] (Figure 1A,B). Briefly, Wistar Albino rats (6 months old, male) were euthanized using a protocol approved by Clinical Research Ethics Committee, Faculty of Medicine, Canakkale Onsekiz Mart University (Permission number: 2016/02-08). The dissected brains were cut under a dissection microscope from ventral to dorsal between the left striatum and the left ventricle. Finally, SVZ-tissues were dislodged with a cut at the dorsal SVZ along the *corpus callosum*. The dislodged SVZ tissues were kept in Hibernate A medium (Thermo Fisher, USA), a CO_2-independent medium for the maintenance of neural cells until further processed for NSCs isolation.

For NSC isolation, the SVZ tissues were dissociated by pipetting, followed by treatment with trypsin–EDTA (0.05%) in Neurobasal A (Thermo Fisher, USA). After centrifugation, the obtained cell pellet was resuspended in N2B27 medium consisting of Neurobasal/DMEM-F12 (1:1) supplemented with GlutaMax (0.5% v/v), penicillin/streptomycin (1% v/v), EGF (10 ng mL^{-1}), bFGF (20 ng mL^{-1}), N2 (1% v/v) and B27 (2% v/v). All media and supplements were obtained from Thermo Fisher, USA. The cells were then plated on Laminin-coated 6-wells (2×10^5 cells $well^{-1}$).

Various techniques were used for the detailed characterization of the isolated cells. For the phenotypical analysis of rNSCs with flow cytometry, cells (1×10^6) were permeabilized with Triton X-100, blocked with bovine serum albumin (5%, BSA, Sigma-Aldrich, USA) in phosphate buffer saline (PBS), stained with Nestin antibody (1:200, Ab92391, Abcam, USA) and goat anti-rabbit IgG (1:1000, ab72465, Abcam, USA). Flow cytometry (FACSAria, BD, USA) was used to analyze the stained cells.

Expression of Nestin and PAX6 in rNSCs, hMSCs (negative control), and rSVZ tissue (positive control) was investigated by RT-qPCR (primers are listed in the Supporting Information). Total RNA was isolated from rNSCs, hMSCs, and rSVZ tissue using a commercial RNA isolation kit (GeneAll, Korea). 100 ng of RNA was measured on a Nanodrop (Nanodrop 2000/2000c, Thermo Fisher, UK) and reverse transcribed using a cDNA synthesis kit (Bio-Rad, USA) to obtain cDNA for each sample. For RT-qPCR, each reaction was run (Bio-rad CFX96 qPCR system, USA) in triplicate using SYBR green master mix, and the gene expressions were normalized to an internal control GAPDH.

The rNSCs were further characterized morphologically by IF staining. The rNSCs were fixed with paraformaldehyde (PFA, 4% v/v), permeabilized with Triton X-100 (0.1% v/v), blocked with BSA (2% v/v), incubated with Nestin antibody (1:200), and finally labeled with goat anti-rabbit IgG secondary antibody with green fluorescence dye (Thermo Fisher, UK). The cell nuclei were stained with DAPI and cells were observed under a fluorescence microscope (Leica DMIL model, Leica, Germany).

The capability of rNSCs to form neurosphere by culturing the cells in ultra-low attachment 96-well plates (ULAP, Corning) for 3–4 days was accessed. In this case, cells (2×10^4) were seeded in N2B27 medium, and the formation of neurospheres was observed under an inverted phase/contrast microscope (Leica, Germany).

Isolation and Characterization of rSVZ-NSCExo: Conditioned media (CM) were collected from NSCs that we cultured up to four passages in laminin-coated 6-well plates in N2B27 medium. Exosomes from rSVZ-NSCs were isolated as described previously[23], but with a slight modification (Figure 2A). The collected CM was centrifuged for 15 min at 300 g and at 4 °C to remove the cells. After filtration through 0.22 µm, CM was centrifuged at 2000 g and 12 000 g at 4 °C to remove apoptotic bodies, microvesicles, and cell debris. Finally, CM was ultracentrifuged for 3 h at 120 000 g and 4 °C to pelletize the exosomes. The isolated exosomes were resuspended in PBS (10 mL) and re-pelletized to remove contaminants. The final product was dispersed in 100 µL of DPBS.

The rSVZ-NSCs derived exosomes were characterized with several techniques. Total protein was extracted from the rSVZ-NSCExo using a radioimmunoprecipitation assay (RIPA) buffer (Thermo Fisher, USA), and protein content was measured using a bicinchoninic acid (BCA) test (Thermo Fisher, USA) by recording the absorbance at 562 nm. For Western Blot (WB) analysis, the extracted proteins were separated by sodium dodecyl sulphate polyacrylamide gel (SDS-PAGE) electrophoresis, subsequently, transferred onto polyvinylidene difluoride (PVDF) membrane. The membrane was then blotted with exosome-specific antibodies namely CD9 and CD63 (1:200, Santa Cruz, USA), which was followed by incubation with horseradish peroxidase-conjugated anti-mouse IgG (1:2000, Abcam, UK). Proteins were then visualized using SuperSignal West Femto electrochemiluminescence (ECL) substrate (Bio-Rad, USA).

To analyze the morphological characteristics, rSVZ-NSCExo was counterstained and examined under TEM. To this end, exosomes suspended in paraformaldehyde were pipetted (4% v/v, 10 µL) onto the formvar-coated copper grids, allowed to settle by incubating for 10 min, further fixed with glutaraldehyde (1%, v/v) and stained with uranyl acetate (1%, w v^{-1}). After each step, the grid was washed with DPBS three times to remove remnants. Images were obtained using transmission electron microscopy (JEM100XC, JEOL, Japan). The size distribution of rSVZ-NSCExo was also assessed by DLS, which measures the alterations of scattered light intensity caused by the Brownian motion of the spherical particles. DLS spectra were obtained for rSVZ-NSCExo -that were diluted with DPBS (1:100 v/v)- using a Nanosizer (Malvern Instruments, Malvern, UK). Measurement was performed in triplicate.

Uptake of rSVZ-NSCExo by hMSCs is an important process for an effective cell differentiation. To investigate the cellular uptake of rSVZ-NSCExo, first we labeled the exosomes with PHK67 (Sigma Aldrich, USA) following the user manual, then incubate them with hMSCs culture (in 6-well plate), and finally observed under a fluorescence microscope (Leica DMIL model, Leica, Germany) using a 488 nm excitation wavelength.

miRNA Array and Metabolomics Study to Characterize Molecular Signatures of rSVZ-NSCExo: Multi-omics analyses, including miRNA array and metabolomics to obtain detailed miRNA and metabolite profiles of rSVZ-NSCExo.

To assess the similarity and differences in miRNA content of rSVZ tissue and rSVZ-NSCExo, miRNA microarray was conducted. rSVZ and exosomal miRNAs were extracted using miRNeasy Mini Kit (Qiagen, USA) in accordance with the manufacturer's instructions. The concentrations of miRNAs were measured with a spectrometer and the integrities were assessed using a Bioanalyzer (Agilent Technologies, USA). The miRNA profiles were obtained on an Affymetrix GeneChip miRNA 4.0 Array (Thermo Fisher, USA) having the capability to recognize 728 rat miRNAs. To examine the metabolite profiles of rSVZ-NSCExo, we extracted metabolites from SVZ-NSCExo and subjected to metabolomics analysis. Sample preparation and derivatization protocols are provided in the Supporting Information. The extracted metabolite samples were analyzed using a GC-MS system (GC-MS-QP-2010 Ultra system, Shimadzu, Japan) with a DB5-MS column as well as LC-qTOF-MS with a C18 column (Agilent 6530, Agilent Technologies, USA).

Investigation of Cytocompatibility of rSVZ-NSCExo: To assess the potential applicability of rSVZ-NSCExo as a cell induction agent, Calcein-AM/EthD-1 staining was conducted to examine the cell viability

before proceeding with further experiments. For this purpose, hMSCs were seeded in 96-well plates (7.5×10^3 cells well^{-1}) in a commercial expansion medium (Merck Millipore, USA) with exosome-depleted fetal bovine serum (FBS, 10% v/v) (System Biosciences, USA) and penicillin/streptomycin (1%, v/v). Various concentrations (10, 50, and 100 μg mL^{-1}) of rSVZ-NSCExo were injected into the media 1 day after cell seeding. After definite culture periods (2 and 7 days), media were replaced with Calcein-AM/EthD-1 solution (4 μM, Molecular Probes, Thermo Fisher, UK), and cell viability was observed under a fluorescence microscope (Leica DMIL model, Leica, Germany) using green (ex. 488 nm) and red (ex. 527 nm) channels. In addition, MTS testing was conducted to investigate the effect of rSVZ-NSCExo on cell proliferation. These experiments were conducted with the same exosome concentrations and in the same conditions with the cell viability assay. After definite time points (2 and 7 days), the waste medium was discarded, and 20 μL of MTS reagent was added in each well containing 100 μL of fresh culture medium. After 1 h incubation in the dark at 37 °C, absorbance values were recorded at 490 nm. Each parameter was studied in triplicate. Tukey's multiple comparison test was used for the statistical evalution and comparison of groups.

rSVZ-NSCExo Mediated Induction of hMSCs: The neuro-inductive potential of rSVZ-NSCExo on hMSCs was assessed by seeding cells in 6-well plates (5×10^4 cell well^{-1}) in the presence DMEM medium supplemented with FBS (10%, v/v) and P/S (1%, v/v) (denoted as growth medium, GM), and cultured for 1 day in order to ensure cell adhesion and spreading. On the following day, the media were discarded and replaced with DMEM medium with exosome-depleted FBS (2%, v/v) which was supplemented with rSVZ-NSCExo in different concentrations (10, 50, 100 μg mL^{-1}). Here, hMSCs that were cultured in GM and N2B27 medium were used as negative and positive controls, respectively.

The potential of rSVZ-NSCExo to induce hMSCs into neural-lineage cells was investigated phenotypically with IF staining. hMSCs, that were induced with rSVZ-NSCExo (10, 50, and 100 μg mL^{-1}) for 10 days, were immunostained with antibodies Nestin (1:200, Abcam, USA), SOX2 (1:200, Abcam, USA), GFAP (1:200, Thermo Fisher, USA), and vimentin (1:200, Santa Cruz Biotechnology, USA) following the method described in the Section 4.1. Following secondary staining with goat anti-mouse IgG or goat anti-rabbit IgG, cells were observed under a fluorescence microscope (Leica DMIL model, Leica, Germany). To further assess the neuro-inductive potential of rSVZ-NSCExo, expressions of Nestin, GFAP, SOX2, PAX6, and Nestin in rSVZ-NSCExo induced hMSCs were investigated by RT-qPCR following the protocol described in the Section 4.1 (primers have been listed in Supporting Information). In this case, hMSCs cultured in GM were used as the negative control, while hMSCs cultured in N2B27 were considered as the positive control. The differences between expression levels among groups were evaluated with a one-way ANOVA test; p-values < 0.05 were considered significant.

Optimization of the Exosome-Mediated Neurogenic Differentiation Approach: To optimize the rSVZ-NSCExo based cell induction protocol, the effects of initial cell density and exosome loading frequency were investigated. For this purpose, rSVZ-NSCExo (100 μg mL^{-1}) was injected into the 6-wells in which hMSCs were cultured in different cell densities (5×10^4, 1×10^5, and 2×10^5 cells per 6-well). Culture media were refreshed every 3 days. To assess the effect of the exosome loading frequency, rSVZ-NSCExo (100 μg mL^{-1}) was loaded to the cell culture (5×10^4 cell per 6-well) 1, 2, and 3 times with 3-days' intervals. At the end of the 10-day induction period, neurogenic gene expressions were investigated with RT-qPCR for Nestin, SOX2, PAX6, GFAP, MAP2, and vimentin. The differences between expression levels among groups were evaluated with a one-way ANOVA test; p-values < 0.05 were considered significant.

Assessment of rSVZ-NSCExo-Mediated Induction Strategy Using Multi-Omics Approach: miRNA Profiling and Metabolomics: Mechanism of action of the rSVZ-NSCExo mediated induction of hMSCs into neural-lineage cells was deeply investigated with a multi-omics approach, including miRNA array and metabolomics. In this case, miRNA profile of hMSCs was compared with the miRNA profile of rSVZ-NSCExo (100 μg mL^{-1})-induced hMSCs. In addition, metabolomics patterns of hMSCs induced with different concentrations of rSVZ-NSCExo (10, 50, and 100 μg mL^{-1}) were obtained. For a time-resolved mechanical understanding, metabolomics analyses for 1, 3, 5, and 10-days of exosomal induction were also performed. miRNA array and metabolomics analyses were performed as described in the Section 4.3. Additional notes on sample preparation and processing were provided in Supporting Information.

Statistical Analysis and Bioinformatics: Throughout the work, quantitative experiments were conducted in triplicate. Statistical evaluation and comparison of groups in MTS testing were analyzed with Tukey's multiple comparison test. In RT-qPCR studies, the differences between expression levels among groups were evaluated with a one-way ANOVA test; p-values < 0.05 were considered significant. Statistical analyses were performed by OriginPro 2021.

Deconvolution, peak alignment, and metabolite identification were carried out with MS-DIAL (ver. 4.48) software for the metabolomic data. Peak annotations were done in GC-MS using retention index libraries. For LC-qTOF-MS based metabolomic analysis, formula predictions, and structure elucidations by means of unknown spectra were done by querying the acquired MS/MS data against the Human Metabolome Database (HMDB), Lipid Maps, Chemical Entities of Biological Interest (ChEBI), and PubChem with MS-Finder (ver. 3.50) software. TIC normalization was done for raw data set and mean scaling was applied to identified metabolite list in each group. Statistical analysis was carried out in Metaboanalyst 5.0 and 50% of the values missing were excluded from the data matrix, and PLS-DA, heatmap, one-way ANOVA, and pathway impact plots were created.

Acknowledgements

This work was financially supported by the Scientific and Technological Research Council of Turkey (TUBITAK) with the grant number 116S476.

Conflict of Interest

The authors declare no conflict of interest.

Author Contributions

B.D. and E.E. conceived and designed the study. B.D. and I.E., dissected SVZ tissues from rats. B.D. and Y.E.A. isolated and characterized NSCs. B.D. and M.I. performed in vitro cell culture experiments. C.C., S.B., and M.A. performed exosome isolation and characterization. F.K. supervised gene expression study. C.C.C. and E.N. performed metabolomics and bioinformatics studies. O.A. and Ç.E. supervised exosome isolation and characterization. B.O.O. made data curing, reviewed and revised the manuscript.

Data Availability Statement

The data that support the findings of this study are available from the corresponding author upon reasonable request.

Keywords

exosomes, extracellular vesicles, mesenchymal stem cells, metabolomics, neural differentiation, neural stem cells, subventricular zone

Received: December 9, 2021
Revised: March 2, 2022
Published online: March 28, 2022

[1] D. Y. Kim, I. Hwang, F. L. Muller, J. H. Paik, *Cell Death Differ.* **2015**, *22*, 2034.
[2] X. Li, W. Zhou, X. Li, M. Gao, S. Ji, W. Tian, G. Ji, J. Du, A. Hao, *Stem Cell Res. Ther.* **2019**, *10*, 389.
[3] D. R. Kaplan, F. D Mille, *Curr. Opin. Neurobiol.* **2000**, *103*, 381.
[4] J. Wang, H. Cheng, X. Li, W. Lu, K. Wang, T. Wen, *Mol. Neurobiol.* **2013**, *47*, 228.
[5] S. Bel-Vialar, F. Medevielle, F. Pituello, *Dev. Biol.* **2007**, *305*, 659.
[6] M. A. Kahn, C. J. Huang, A. Caruso, V. Barresi, R. Nazarian, D. F. Condorelli, J. de Vellis, *J. Neurochem.* **1997**, *68*, 1413.
[7] S. K. Zahr, D. R. Kaplan, F. D. Miller, *Cell Death Differ.* **2019**, *26*, 2495.
[8] A. Baser, M. Skabkin, S. Kleber, Y. Dang, G. S. Gülcüler Balta, G. Kalamakis, M. Göpferich, D. C. Ibañez, R. Schefzik, A. S. Lopez, E. L. Bobadilla, C. Schultz, B. Fischer, A. Martin-Villalba, *Nature* **2019**, *566*, 100.
[9] J. Han, H. J. Kim, S. T. Schafer, A. Paquola, G. D. Clemenson, T. Toda, J. Oh, A. R. Pankonin, B. S. Lee, S. T. Johnston, A. Sarkar, A. M. Denli, F. H. Gage, *Neuron* **2016**, *91*, 79.
[10] K. E. Szulwach, X. Li, R. D. Smrt, Y. Li, Y. Luo, L. Lin, N. J. Santistevan, W. Li, X. Zhao, P. Jin, *J. Cell. Biol.* **2010**, *189*, 127.
[11] J. O. Brett, V. M. Renault, V. A. Rafalski, A. E. Webb, A. Brunet, *Aging* **2011**, *3*, 108.
[12] A. de Chevigny, N. Coré, P. Follert, M. Gaudin, P. Barbry, C. Béclin, H. Cremer, *Nat. Neurosci.* **2012**, *15*, 1120.
[13] D. Woodbury, E. J. Schwarz, D. J. Prockop, I. B. Black, *J. Neurosci. Res.* **2000**, *61*, 364.
[14] Y. Hu, Y. Zhang, K. Tian, C. Xun, S. Wang, D. Lv, *Mol. Med. Rep.* **2016**, *13*, 49.
[15] J. Sanchez-Ramos, S. Song, F. Cardozo-Pelaez, C. Hazzi, T. Stedeford, A. Willing, T. B. Freeman, S. Saporta, W. Janssen, N. Patel, D. R. Cooper, P. R. Sanberg, *Exp. Neurol.* **2000**, *164*, 247.
[16] W. Deng, M. Obrocka, I. Fischer, D. J Prockop, *Biochem. Biophys. Res. Commun.* **2001**, *282*, 148.
[17] Y. Lu, X. Yuan, Y. Ou, Y. Cai, S. Wang, Q. Sun, W. Zhang, *Neural Regener. Res.* **2012**, *7*, 1205.
[18] M. Bahls, S. Könemann, M. R. P. Markus, K. Wenzel, N. Friedrich, M. Nauck, H. Völzke, A. Steveling, D. Janowitz, H. J. Grabe, S. B. Felix, M. Dörr, *Sci. Rep.* **2019**, *9*, 15421.
[19] L. Aloe, M. L. Rocco, P. Bianchi, L. Manni, *J. Transl. Med.* **2012**, *10*, 239.
[20] Y. J. Jung, H. K. Kim, Y. Cho, J. S. Choi, C. H. Woo, K. S. Lee, J. H. Sul, C. M. Lee, J. Han, J. H. Park, D. G. Jo, Y. W. Cho, *Sci. Adv.* **2020**, *6*, 6721.
[21] R. Upadhya, L. N. Madhu, S. Attaluri, D. L. G. Gitaí, M. R. Pinson, M. Kodali, G. Shetty, G. Zanirati, S. Kumar, B. Shuai, S. T. Weintraub, A. K. Shetty, *J. Extracell. Vesicles* **2020**, *9*, 1809064.
[22] Y. Men, J. Yelick, S. Jin, Y. Tian, M. S. R. Chiang, H. Higashimori, E. Brown, R. Jarvis, Y. Yang, *Nat. Commun.* **2019**, *10*, 4136.
[23] C. C. Eylem, M. Yilmaz, B. Derkus, C. B. Camci, E. Nemutlu, E. Yilmaz, M. A. Turkoglu, B. Aytac, N. Ozyurt, E. Emregul, *Cancer Lett.* **2020**, *469*, 186.
[24] Z. G. Zhang, B. Buller, M. Chopp, *Nat. Rev. Neurol.* **2019**, *15*, 193.
[25] G. van Niel, G. D'Angelo, G. Raposo, *Nat. Rev. Mol. Cell Biol.* **2018**, *19*, 213.
[26] K. D. Sharmai, D. Schaal, R. A. Kore, R. N. Hamzah, S. C. Pandanaboina, A. Hayar, R. J. Griffin, M. Srivatsan, N. S. Reyna, J. Y. Xie, *PLoS One* **2000**, *15*, e0234614.
[27] K. C. S. Roballo, J. C. da Silveira, F. F. Bressan, A. F. de Souza, V. M. Pereira, J. E. P. Porras, F. A. Rós, L. H. Pulz, R. de Francisco-Strefezzil, D. dos Santos-Martins, F. V. Meirelles, C. E. Ambrósio, *Sci. Rep.* **2019**, *9*, 11213.
[28] Y. S. Takeda, Q. Xu, *PLoS One* **2015**, *10*, e0135111.
[29] K. Narayanan, S. Kumar, P. Padmanabhan, B. Gulyas, A. C. A. Wan, V. M. Rajendran, *Biomaterials* **2018**, *182*, 312.
[30] W. R. Lan, S. Pan, H. Y. Li, C. Sun, X. Chang, K. Lu, C. Q. Jiang, R. Zuo, Y. Zhou, C. Q. Li, *Stem Cells Int.* **2019**, *2019*, 8404168.
[31] C. C. Huang, R. Narayanan, S. Alapati, S Ravindran, *Biomaterials* **2016**, *111*, 103.
[32] Y. Ma, C. Li, Y. Huang, Y. Wang, X. Xia, J. C. Zheng, *Cell Commun. Signaling* **2019**, *17*, 96.
[33] Y. Rong, W. Liu, J. Wang, J. Fan, Y. Luo, L. Li, F. Kong, J. Chen, P. Tang, W. Cai, *Cell Death Dis.* **2019**, *10*, 340.
[34] M. C. Morton, V. N. Neckles, C. M. Seluzicki, J. C. Holmberg, D. M. Feliciano, *Cell Rep.* **2018**, *23*, 78.
[35] A. Lee, J. D. Kessler, T. A. Read, C. Kaiser, D. Corbeil, W. B. Huttner, J. E. Johnson, R. J. Wechsler-Reya, *Nat. Neurosci.* **2005**, *8*, 723.
[36] S. Jmorrison, P. M. White, C. Zock, D. J. Anderson, *Cell* **1999**, *96*, 737.
[37] A. Liu, X. Chen, L. Bao, T. Liu, P. Yuan, X. Yang, X. Qui, J. J. Gooding, Y. Bai, J. Xiao, F. Pu, Y Jin, *Nat. Biomed. Eng.* **2020**, *4*, 1063.
[38] W. Du, K. Zhang, S. Zhang, R. Wang, Y. Nie, H. Tao, Z. Han, L. Liang, D. Wang, J. Liu, N. Liu, Z. Han, D. Kong, Q. Zhao, Z. Li, *Biomaterials* **2017**, *133*, 70.
[39] H. Kim, J. Y. Kang, D. Mun, N. Yun, B. Joung, *PLoS One* **2017**, 14.
[40] G. Zhang, Z. Zhu, H. Wang, Y. Yu, W. Chen, A. Waqas, Y. Wang, L. Chen, *J. Adv. Res.* **2020**, *24*, 435.
[41] S. Yang, S. Guo, S. Tong, X. Sun, *Stem Cells Int.* **2019**, *2019*, 1351860.
[42] G. U. Höglinger, P. Rizk, M. P. Muriel, C. Duyckaerts, W. H. Oertel, I. Caille, E. C. Hirsch, *Nat. Neurosci.* **2004**, *7*, 726.
[43] A. S. Peden, P. Mac, Y. J. Fei, C. Castro, G. Jiang, K. J. Murfitt, E. A. Miska, J. L. Griffin, V. Ganapathy, E. M Jorgensen, *Nat. Neurosci.* **2013**, *16*, 1794.
[44] M. Ko, K. Zou, H. Minagawa, W. Yu, J. S. Gong, K. Yanagisawa, M. Michikawa, *J. Biol. Chem.* **2005**, *280*, 42759.
[45] D. H. Mauch, K. Nägler, S. Schumacher, C. Göritz, E. C. Müller, A. Otto, F. W. Pfrieger, *Science* **2001**, *294*, 1354.
[46] C. W. Lee, T. V. Lee, V. C. Chen, S. Bui, S. Riechman, *FASEB J.* **2011**, *25*, 563.
[47] W. Kilb, A. Fukuda, *Front. Cell. Neurosci.* **2017**, *11*, 328.
[48] Y. J. Jun, H. K. Kim, Y. Cho, J. S. Choi, C. H. Woo, K. S. Lee, J. H. Sul, C. M. Lee, J. Han, J. H. Park, D.-G. Jo, Y. W Cho, *Sci. Adv.* **2020**, *6*, eaay6721.
[49] Y. Ma, C. Li, Y. Huang, Y. Wang, X. Xia, J. C. Zheng, *Cell Commun. Signaling* **2019**, *17*, 96.
[50] E. Stronati, R. Conti, E. Cacci, S. Cardarelli, S. Biagioni, G. Poiana, *Int. J. Mol. Sci.* **2019**, *20*, 3691.
[51] Q. Mao, P. D. Nguyen, R. M. Shanti, S. Shi, P. Shakoori, Q. Zhang, A. D Le, *Tissue Eng., Part A* **2019**, *25*, 887.
[52] P. Yuan, L. Ding, H. Chen, Y. Wang, C. Li, S. Zhao, X. Yang, Y. Ma, J. Zhu, X. Qi, Y. Zhang, X. Xia, J. C. Zheng, *Front. Cell Dev. Biol.* **2021**, *9*, 601660.
[53] Y. Men, J. Yelick, S. Jin, Y. Tian, M. S. R. Chiang, H. Higashimori, E. Brown, R. Jarvis, Y. Yang, *Nat. Commun.* **2019**, *10*, 4136.
[54] H. K. Wilson, S. G. Canfield, M. K. Hjortness, S. P. Palecek, E. V Shusta, *Fluids Barriers CNS* **2015**, *12*, 13.
[55] D. Grimm, K. L. Streetz, C. L. Jopling, T. A. Storm, K. Pandey, C. R. Davis, P. Marion, F. Salazar, M. A. Kay, *Nature* **2006**, *441*, 537.
[56] R. Kintaka, K. Makanea, H. Moriya, *Sci. Rep.* **2016**, *6*, 31774.
[57] D. Ron, *Science* **2006**, *313*, 52.
[58] J. Liu, J. Githinji, B. Mclaughlin, K. Wilczek, J Nolta, *Stem Cell Rev. Rep.* **2012**, *8*, 1129.
[59] T. K. Ng, Q. Yang, V. R. Fortino, N. Y. Lai, C. M. Carballosa, J. M. Greenberg, K. W. Choy, D. Pelaez, C. P. Pang, H. S. Cheung, *J. Tissue Eng. Regener. Med.* **2019**, *13*, 12.
[60] L. Stappert, L. Borghese, B. Roese-Koerner, P. Weinhold, S. Koch, M. Terstegge, S. Uhrberg, P. Wernet, O Brüstle, *PLoS One* **2013**, *8*, 10.
[61] X. H. Parsons, J. F. Parsons, D. A. Moore, *Mol. Med. Ther.* **2012**, *1*, 105.

[62] Z. J. Wei, B. O. Fan, Y. Liu, H. Ding, H. S. Tang, D. Y. Pan, J. Shi, P. Zheng, H. Shi, H. Wu, A. Li, S. Feng, *Neural Regener. Res.* **2019**, *14*, 1462.
[63] M. Kang, S. Park, J. Han, *Cell. Mol. Life Sci.* **2019**, *76*, 4569.
[64] L. Pereira, R. Medina, M. Baena, A. M. Planas, E. Pozas, *Front. Cell Neurosci.* **2015**, *9*, 270.
[65] K. Warre-Cornish, L. Perfect, R. Nagy, R. R. R. Duarte, M. J. Reid, P. Raval, A. Mueller, A. L. Evans, A. Couch, C. Ghevaert, G. McAlonan, E. Loth, D. Murphy, T. R. Powell, A. C. Vernon, D. P. Srivastava, J. Price, *Sci. Adv.* **2020**, *6*.
[66] A. Y. Galvez-Contreras, A. Quiñones-Hinojosa, O. Gonzalez-Perez, *Front. Cell Neurosci.* **2013**, *7*.
[67] C. Rio, H. I. Rieff, P. Qi, T. S. Khurana, G. Corfas, *Neuron* **1997**, *19*, 39.
[68] M. Abaskharoun, M. Bellemare, E. Lau, R. U. Margolis, *ASN Neuro* **2010**, *2*, AN20100001.
[69] Y. H. Jen, M. Musacchio, A. D. Lander, *Neural Dev.* **2019**, *4*, 33.
[70] K. L. Eagleson, C. J. Lane, L. McFadyen-Ketchum, S. Solak, H. H. Wu, P. Levitt, *Dev. Neurobiol.* **2016**, *76*, 1160.
[71] B. P. Williams, J. K. Park, J. A. Alberta, S. G. Muhlebach, G. Y. Hwang, T. M. Roberts, C. D Stiles, *Neuron* **1997**, *18*, 553.
[72] K. W. Adams, S. Kletsov, R. J. Lamm, J. S. Elman, S. Mullenbrock, G. M. Cooper, *PLoS One* **2017**, *12*, e0170076.
[73] M. Mondanizadeh, E. Arefian, G. Mosayebi, M. Saidijam, B. Khansarinejad, S. M Hashemi, *J. Cell. Biochem.* **2015**, *116*, 943.
[74] M. C. Santos, A. N. Tegge, B. R. Correa, S. Mahesula, L. Q. Kohnke, M. Qiao, M. A. Ferreira, E. Kokovay, L. O. Penalva, *Stem Cells* **2016**, *34*, 220.
[75] A. Ahmad, S. Strohbuecker, C. Tufarelli, V. Sottilev, *Cell. Mol. Life Sci.* **2017**, *74*, 4245.
[76] T. Kondo, A. J. Matsuoka, A. Shimomura, K. R. Koehler, R. J. Chan, J. M. Miller, E. F. Srour, E. Hashino, *Stem Cells* **2011**, *29*, 836.
[77] H. H. Tzeng, C. H. Hsu, T. H. Chung, W. C. Lee, C. H. Lin, W. C. Wang, C. Y. Hsiao, Y. W. Leu, T. H. Wang, *PLoS One* **2015**, *10*, e0145542.
[78] B. Zheng, C. Wang, L. He, X. Xu, J. Qu, J. Hu, H. Zhang, *J. Cell. Physiol.* **2013**, *228*, 149.
[79] R. M. Brick, A. X. Sun, R. S. Tuan, *Stem Cells Transl. Med.* **2018**, *7*, 45.
[80] L. Peng, X. Shu, C. Lang, X. Yu, *Cytotechnology* **2017**, *69*, 933.
[81] M. E. Klontzas, S. I. Vernardis, M. Heliotis, E. Tsiridis, A. Mantalaris, *Stem Cells Dev.* **2017**, *26*, 723.
[82] A. Marin-Navarro, R. J. Pronk, A. T. van der Geest, G. Oliynyk, A. Nordgren, M. Arsenian-Henriksson, A. Falk, M. Wilhelm, *Cell Death Dis.* **2020**, *11*, 52.
[83] S. J. Park, S. A. Lee, N. Prasain, D. Bae, H. Kang, T. Ha, J. S. Kim, K. S. Hong, C. Mantel, S. H. Moon, H. E. Broxmeyer, M. R Lee, *Stem Cells Dev.* **2017**, *26*, 734.
[84] R. Jellali, M. L. Bernier, Y. Tauran, F. Gilard, M. Danov, T. Kido, A. Miyajima, Y. Sakai, E Leclerc, *Differentiation* **2020**, *112*, 17.
[85] A. Kumar, Y. Kumar, J. K. Sevak, S. Kumar, N. Kumar, S. D. Gopinath, *Sci. Rep.* **2020**, *10*, 10.
[86] M. C. Morton, V. N. Neckles, D. M. Feliciano, *Methods Mol. Biol.* **2018**, *2002*, 75.
[87] W. Guo, N. E. Patzlaff, E. M. Jobe, X. Zhao, *Nat. Prot.* **2012**, *7*, 2005.